Chemical Methodologies 6(2022) 886-904

Chemical Methodologies

Journal homepage: http://chemmethod.com

Original Research Article

Design and Construction of a Novel and an Efficient Potentiometric Sensor for Determination of Sodium Ion in Urban Water Samples

Shiva Ariavand[1], Mahmoud Ebrahimi[1,*], Ebrahim Foladi[1,2,*]

[1]Department of Chemistry, Mashhad Branch, Islamic Azad University, Mashhad, Iran
[2]Department of Food Safety and Quality Control, Research Institute of Food Science and Technology (RIFST), Mashhad, Iran

ARTICLE INFO

Article history
Submitted: 2022-04-23
Revised: 2022-07-15
Accepted: 2022-08-15
Manuscript ID: CHEMM-2206-1567
Checked for Plagiarism: **Yes**
Language Editor:
Dr. Ermia Aghaie
Editor who approved publication:
Dr. Zeinab Arzehgar

DOI:10.22034/CHEMM.2022.348712.1567

KEYWORDS
Sodium-ion
Modified sensor
Graphene oxide
Ionic Liquid
1, 4 Diaminoanthraquinone
Experimental design

ABSTRACT

Sodium ions are one of the essential cations for various activities in the human body to control fluid levels, blood pressure, and nerve and muscle functions. Sodium-ion is a highly soluble chemical that small amounts of it can be absorbed by the body through water intake. However, consuming an excess amount of sodium ions can cause problems in the body. Therefore, it is vital to measure sodium ions in water samples. A novel and cheap potentiometric sensor was developed to measure trace amounts of sodium ions in real water samples. For the purpose, four effective components in the Nernstian response of the sensor, including 1-Hexyl-3-methyl imidazolium hexafluorophosphate as an ionic liquid, 1, 4 Diaminoanthraquinone (DAQ) as an ionophore, graphene oxide nanosheets, and paraffin oil as a binder were optimized using a response surface methodology (RSM) based on central composite design. The optimum percentages of paraffin, ionic liquid, ionophore, and graphene oxide to prepare the sensor were 13.34, 11.40, 3.21, and 2.16 %, respectively. Under the best percentage of electrode components, the potentiometric sensor showed a suitable slope of 59.2 mV decade^{-1} over a wide Na^+ concentration range (10^{-6}-10^{-2} mol L^{-1}) with a proper detection limit of 8.97×10^{-7} mol L^{-1}. The sensor can be applied to measure sodium ions in a pH range of 4 to 8. The optimized geometry of the complex formed between sodium ion and the ionophore was investigated using the density functional theory (DFT) methods.

GRAPHICAL ABSTRACT

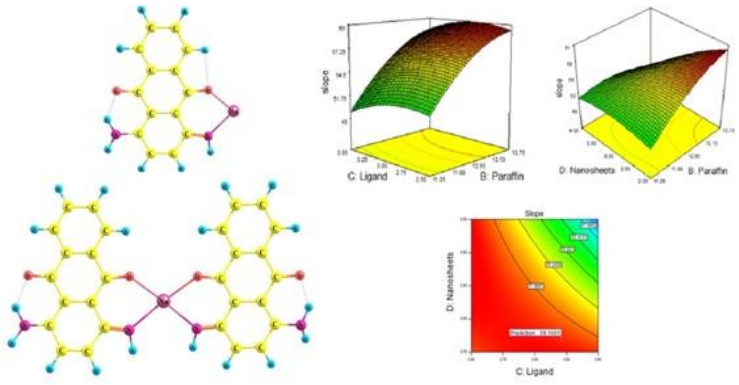

* Corresponding author: Mahmoud Ebrahimi
✉ E-mail: : ebrachem2007@yahoo.com , e.fooladi@rifst.ac.ir

Introduction

Carbon paste electrodes (CPE_s) have been extensively utilized in electroanalysis because of possessing unique properties such as low cost, wide potential window, and proper sense diversity [1]. Other advantages of CPE to determine an analyte include simple and fast fabrication, rapid response, low residual current, renewable surface, simple maintenance, and suitable selectivity [2, 3]. The performance of CPE_s for an analyte determination is contingent upon the properties of the modifier materials present in its components [4-9]. One type of new working electrode is the ionic liquid-carbon paste electrode (IL-CPEs), which is fabricated using an ionic liquid as the modifier and binder in the traditional CPE_s [10, 11]. The unique properties of ionic liquids such as low vapor pressure, high ionic conductivity, negligible toxicity, wide electrochemical windows, and high thermal stability have resulted, leading to an intrinsic electrocatalytic ability and wide electrochemical windows in IL–CPEs [12-15].

Sodium-ion is known as one of the main extracellular fluid cations [16]. These ions are involved in the regulation of regulate the acid-base balance in the kidneys by replacing hydrogen ions with sodium ions in the renal tubule [17, 18]. Besides, the sodium ion is a vital electrolyte in the body, and its balance dramatically impacts human health. Obviously. Electrolyte plays an essential role in most metabolic processes. Increasing levels of this electrolyte in the body can cause excess fluid, tissue swelling, and reduced urine output [19]. Age, stress, sodium intake, and water mineralization can contribute to the development of primary hypertension. Among the factors mentioned, sodium intake is a significant parameter with a high effect on primary hypertension [20]. In the diet, a small amount of sodium can be absorbed into the body through water intake [21, 22]. Thus, determining Na^+ ions in real water samples is critical for evaluating their effects on the human body.

Meanwhile, graphene oxide (GO) is a two-dimensional nanosheet synthesized from the oxidation of graphite powder using a chemical procedure based on the Hummers' method [23]. GO sheets are used as a modifier in the preparation of electrochemical sensors due to their interesting physicochemical properties such as high thermal and chemical stability, large surface area, and good electron mobility [24-26].

The response surface is a plot in two or three dimensions, describing the relationship between the response and one or more factor levels. Response surface methodology (RSM) describes the response surfaces of experimental design with information about systems. RSM is a collection of mathematical methods that investigates investigating the relationship between one or several response variables and several independent variables [27, 28]. Design of Experiments (DOE) is a branch of statistics that investigates the effect of changes in input variables (Xs) on the outputs response variable (Y). Another traditional method to study these effects is one factor at a time (OFAT), in which the effect of one factor on the response is investigated while. In contrast, the other factors are fixed in certain values. Disadvantages of the strategy are the a large number of experiments and the absence of the possibility of simultaneous examination of variables and their interactions [29]. Nevertheless, in the DOE method, the effect of changing all the factors is simultaneously studied in the response, which leads to a reduction in the number of experiments and the study of the effects of the interaction between the factors [30].

In the present study, a new selective and sensitive CPE was developed using 1-Hexyl-3-methylimidazolium hexafluorophosphate and graphene oxide nanosheets to determine the trace amounts of sodium ions in real water samples. Also, the percentage of the CPE components, including 1-Hexyl-3methyl imidazolium hexafluorophosphate as an ionic liquid, 1, 4 Diaminoanthraquinone (DAQ) as an ionophore, graphene oxide nanosheets, and paraffin oil as a binder were optimized using a response surface methodology (RSM) based on central composite design. Using a proper ionic liquid and a suitable ligand in the sensor construction leads to an

increase in the method's selectivity, a reduction in the response time, and an increase in the sensor's lifetime for measuring sodium ions. Besides, the application of applying graphene oxide nanosheets as a sensor component can enhance the sensor quality with its convenient properties such as high thermal and chemical stability, large surface area, and good electron mobility. 1, 4 Diaminoanthraquinone is a low price compound used in cosmetics for hair dyeing. A simulation strategy using DFT was performed to check the possibility of interaction between sodium ions and ionophores before preparing the sensor. It exhibits a suitable ability as an ionophore with proper selectivity toward sodium ions in the sensor composite.

Materials and Methods

The stock solution of 0.1 mol L^{-1} of sodium ion was prepared by dissolving a calculated amount of sodium nitrate (0.8499 g) in 100 mL of deionized (DI) water. The working solutions were made up daily by diluting the stock solution of the sodium ion with DI water. DI water was obtained using a Milli-Q purification system (Milford, MA, USA) and was used to prepare all solutions. Graphene oxide nanosheets were purchased from the Research Institute of Petroleum Industry (Tehran, Iran). Also, 1-hexyl-3-methyl imidazolium hexafluorophosphate [C_6MIM] [PF_6] (Purity of 99 %) was purchased from Green Compounds Co. Iran. Further, 1, 4 Diaminoanthraquinone (DAQ) (Purity of ≥88.0%) was obtained from Sigma-Aldrich (USA). Finally, other required chemicals such as Graphite powder (Purity of 99.99 %) and nitrate salts of cations (Purity of ≥99 % were purchased from Merck (Darmstadt, Germany).

Fabrication of the electrode

Different percentages of graphite powder, paraffin oil, ionic liquid, ionophore, and graphene oxide nanosheets were utterly mixed in a mortar for 30 minutes to prepare the CPE. Once the material became utterly homogeneous, the obtained paste was carefully inserted into a polypropylene tube. A stainless-steel rod was inserted from the other end of the propylene tube to create an electrical contact. The outer surface of the electrode was flattened by a special glossy paper. The prepared electrode was placed in the air for 24 hours. The CPE was placed in a solution of 1×10^{-3} mol L^{-1} sodium ions for 24 hours to replace the active regions of the ionophore in the electrode with sodium ions. Then, the electrode surface was washed with DI water. After several times of use, it was placed in 10^{-3} mol L^{-1} of ethylene diamine tetraacetic acid (EDTA) for 30 min.

Apparatus and potentiometric measurements

All potentiometric measurements were performed using a pH meter 827 (Metrohm, Switzerland) at 25 ± 0.1 °C. In this work, the potentiometric system consisted of two electrodes, including a saturated calomel reference electrode (Azar electrode, Iran) as the reference electrode and sodium modified carbon paste electrode (MCPE) as the indicator electrode as the following cell:

(Hg|Hg_2Cl_2, KCl (sat d.) || Na^+ ion sample solution | ion-selective electrode (CPE).

For this purpose, the solutions of sodium nitrate were prepared within the concentration range 10^{-10}-10^{-1} mol L^{-1} at 25± 0.1 °C. Subsequently, two of the electrodes, as mentioned above, were placed together in the solutions to measure the potential, where after stabilization ± 1.0 mV, the potential was recorded at the ambient temperature. Then, the calibration curve was plotted by the potential function versus the concentration logarithm of sodium ions.

Experimental design

Four components, including ionophore (1-Hexyl-3-methyl imidazolium hexafluorophosphate), ionic liquid (1-Hexyl-3-methyl imidazolium hexafluorophosphate), paraffin oil, graphene oxide nanosheets were selected to prepare the CPE sensor. Then, a random design was generated using a central composite design to optimize and examine the effect of the percentage of electrode components as independent variables at two levels in the response (The CPE slope). The design

includes 21 random tests with five repetitions at the central point (Tables 1 and 2).

Table 1: The levels of independent variables considered in the central composite design (CCD)

Code	Factors (w/w %)	-a	Low actual	Center	High actual	+a
A	Ionic Liquid	10	11.25	12.5	13.75	15
B	Paraffin	10	11.25	12.5	13.75	15
C	Ligand	2	2.5	3	3.5	4
D	nanosheets	1	2	3	4	5

[a]*Percents are in the electrode*

Table 2: The central composite design (uncoded values) and the obtained experimental results

Run	A (w/w %)	B (w/w %)	C (w/w %)	D (w/w %)	Graphite	Slope	Linear range (log [Na^+])
1	11.25	11.25	2.5	2	73	51.6	-3 to -8
2	13.75	13.75	3.5	2	67	55.8	-2 to -9
3	13.75	11.25	3.5	4	67.5	53.9	-4 to -8
4	12.5	15	3	3	66.5	56.1	-3 to -6
5	13.75	11.25	2.5	4	68.5	58.8	-1 to -5
6[a]	12.5	12.5	3	3	69	55.6	-1 to -7
7[a]	12.5	12.5	3	3	69	55.9	-1 to -7
8[a]	12.5	12.5	3	3	69	55.2	-1 to -7
9	15	12.5	3	3	66.5	53.8	-2 to -5
10	12.5	12.5	4	3	68	49.23	-1 to -6
11[a]	12.5	12.5	3	3	69	55.6	-1 to -7
12	12.5	12.5	3	1	71	46	-1 to -4
13	11.25	11.25	3.5	2	72	50.3	-1 to -5
14[a]	12.5	12.5	3	3	69	55.6	-1 to -7
15	12.5	10	3	3	71.5	43.1	-3 to -7
16	10	12.5	3	3	71.5	59.643	-2 to -5
17	11.25	13.75	2.5	4	68.5	57.8	-1 to -6
18	12.5	12.5	3	5	67	58.2	-1 to -6
19	13.75	13.75	2.5	2	68	45.4	-4 to -7
20	11.25	13.75	3.5	4	67.5	43.4	-2 to -5
21	12.5	12.5	2	3	70	54.5	-3 to -6

A: Amount of Ionic Liquid; B: Amount of Paraffin; C: Amount of Ligand; D: Amount of nanoparticles

Computational details

Herein, all of the calculations were carried out using the B3LYP functional [31] and the 6-311+G(d,p) basis set as implemented in the Gaussian 03 program [32]. The optimized geometries did not show any imaginary frequencies. Thermal corrections were considered in the evaluation of the energies. All structures were visualized using the Chemcraft 1.7 program [33].

Results and Discussion

CPE optimization and analysis of variance

The obtained responses in Table 2 were evaluated with an analysis of variance (ANOVA) at a 95% confidence limit. The effects of variables and their interactions on the slope based on the ANOVA test are presented in Table 3. P-value is a suitable parameter in the ANOVA table to determine the significant factor in the response (Slope) [34]. According to the p-value, the proposed model is a

significant variable because its p-value is lower than 0.05 and the p-value lack of fit is higher than 0.05 at a 95% confidence limit. However, the lack of fit confirms the diversity of data around the fitted model. Lack of fit is a clear criterion for better data matching and model accuracy. If its p-value is greater than 0.05, then it is not significant and the model fitted with the results well. Besides, the p-value of all factors and interactions except for the interaction between the percentage of paraffin and ligand (BC) was less than 0.05, indicating the significant effects of these factors and interactions on the obtained slope.

Table 3: Analysis of Variance (ANOVA)

Source	Sum of Squares	Df	Mean Square	F Value	p-value	Type of effect
Model	503.07	14	35.93	189.6	< 0.0001	Significant
A-Ionic Liquid	17.07	1	17.07	90.07	< 0.0001	Significant
B-Paraffin	84.5	1	84.5	445.86	< 0.0001	Significant
C-Ligand	26.88	1	26.88	141.85	< 0.0001	Significant
D-Nanosheets	74.42	1	74.42	392.68	< 0.0001	Significant
AB	11.56	1	11.56	61	0.0002	Significant
AC	56.18	1	56.18	296.43	< 0.0001	Significant
AD	91.2	1	91.2	481.23	< 0.0001	Significant
BC	0.61	1	0.61	3.19	0.1242	not significant
BD	31.6	1	31.6	166.74	< 0.0001	Significant
CD	100.82	1	100.82	531.98	< 0.0001	Significant
A^2	1.16	1	1.16	6.1	0.0485	Significant
B^2	61.54	1	61.54	324.69	< 0.0001	Significant
C^2	25.08	1	25.08	132.32	< 0.0001	Significant
D^2	22.22	1	22.22	117.22	< 0.0001	Significant
Residual	1.14	6	0.19			
Lack of Fit	0.81	2	0.4	4.85	0.0852	not significant
Pure Error	0.33	4	0.083			
Cor Total	504.21	20				

Std. Dev.	0.44
Mean	53.13
C.V.%	0.82
PRESS	103.94
R-Squared	0.9977
Adj R-Squared	0.9925
Pred R-Squared	0.7939
Final Equation in Terms of Coded Factors:	Slope =+55.64 -1.46* A +3.25* B -1.30 * C +3.05* D +1.70* A * B +2.65* A * C +4.78 * A * D +0.28 * B * C -2.81* B * D -3.55 * C * D +0.21* A^2 -1.57 * B^2 - 1.00 * C^2 -0.94 * D^2
Final Equation in Terms of Actual Factors:	Slope = +197.32211 -42.38135 * Ionic Liquid +19.47905* Paraffin -15.80263* Ligand +10.35247* Nanosheets +1.08800* Ionic Liquid * Paraffin +4.24000* Ionic Liquid * Ligand +3.82000 * Ionic Liquid * Nanosheets +0.44000* Paraffin * Ligand -2.24860* Paraffin * Nanosheets -7.10000* Ligand * Nanosheets +0.13731* Ionic $Liquid^2$ - 1.00213* $Paraffin^2$ -3.99831* $Ligand^2$ -0.94083*

	Nanosheets[2]

To study the effect of the interaction in the slope, the 3D graphical plots are presented in Figure 1, showing that the responses change dramatically with the simultaneous change of factors. Changes in the CPE slope is the greatest in Figure 1**a**, which confirms that the interaction between the ligand and the ionic liquid has the highest effect on the slope. However, the slope increases simultaneously with an increasing percentage of the ligand (C) and a decreasing percentage of the ionic liquid (A) (Figure 1**a**). Similarly, the slope value improved with a low percentage of liquid ionic (A) and a high percentage of paraffin (B) (Figure 1**b**). As shown in Figure 1**d**, the interaction between paraffin (B) and ligand (C) is not significant, and both parameters with the maximum value show better CPE slopes [16]. Figure 1**f** demonstrates the interaction between graphene oxide nanosheets (D) and ligand(C). The slope value approaches the value of the Nernstian slope with increasing ligand percentage [35].

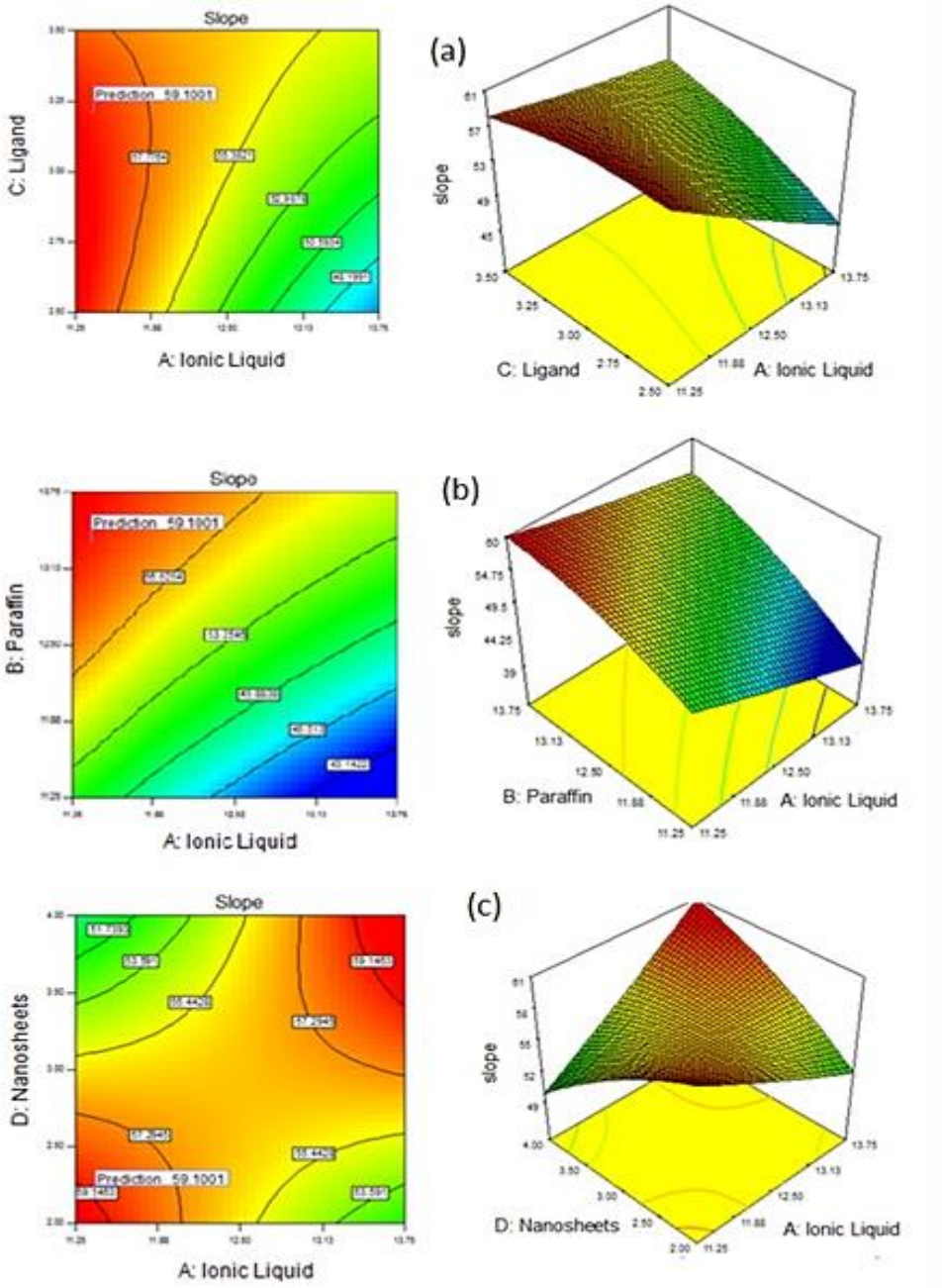

Figure 1a-1c: The response 3D surface plots for interaction effects of variables on the slope: a) AC (interaction of ligand and ionic liquid); b) AB (interaction of paraffin and ionic liquid); c) AD (interaction of nanoparticle and ionic liquid

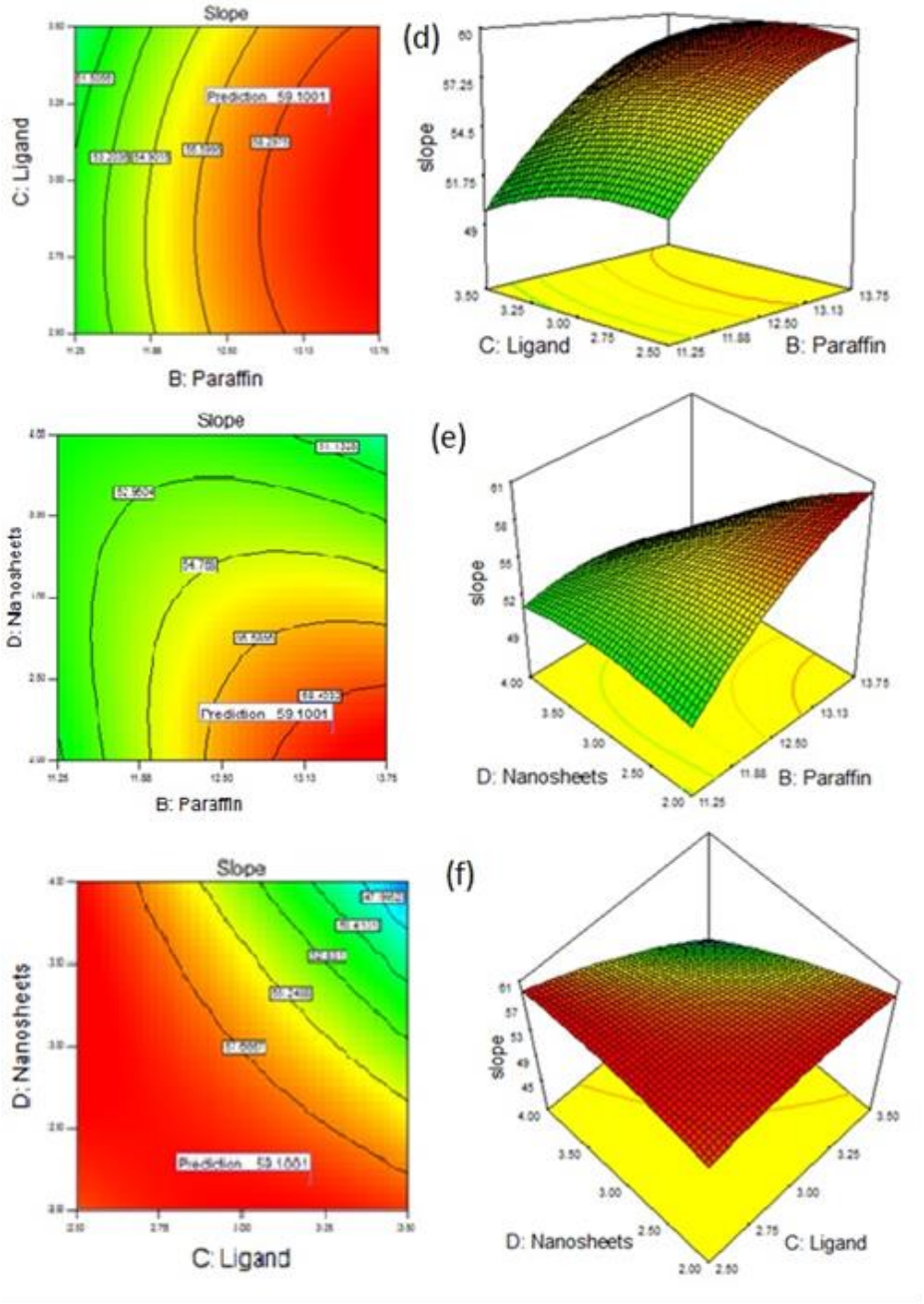

Figure 1d-1f: d) BC (interaction of ligand and paraffin); e) BD (Interaction of paraffin and nanoparticle); f) CD (interaction of nanoparticle and ligand

Figure 1**e** illustrates the interaction between graphene oxide nanosheets (D) and paraffin (B). It indicates that the CPE slope approaches the Nernstian slope with decreasing graphene oxide and increasing paraffin percentage. The quality of the fitting results with the model is described by the coefficient of determination (R^2) and the adjusted coefficient of determination (R^2_{adj}).

The values of R^2 and adjusted R^2 were obtained as 0.9977and 0.9925, respectively (Table 3), showing the model fitted with the responses well. Figure 2 illustrates the diagram of the predicted value of slope versus its actual values**.** According to the Nernst equation, the target Nernstian slope response for the sodium ion is 59.1 mV decade^{-1}. The optimum values with the best desirability for the Nernstian slope were obtained as percentage

of paraffin, ionic liquid, ionophore (ligand), and graphene oxide were 13.34, 11.40, 3.21, and 2.16 %, respectively (Table 4).

Also, the best corresponding electrode response was obtained as 59.2 ± 0.16 mV decade^{-1} under the optimized conditions (Figure 3). Also, linear dynamic range (Figure 4), response time, and detection limit were obtained as 1×10^{-6}-1×10^{-2} mol L^{-1}, 20 Sec, and 8.97×10^{-7} mol L^{-1}, respectively. The reproducibility of the electrode was investigated by the electrode.

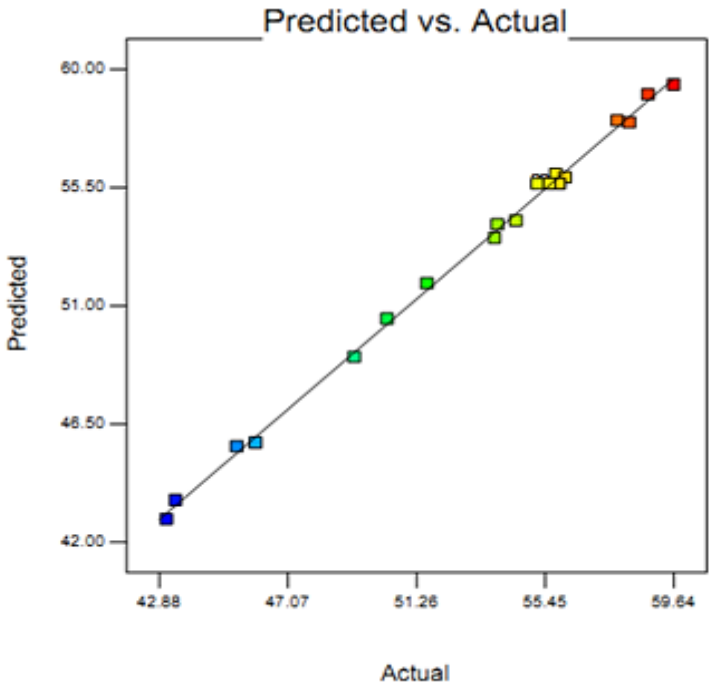

Figure 2: Relationship between predicted versus real values

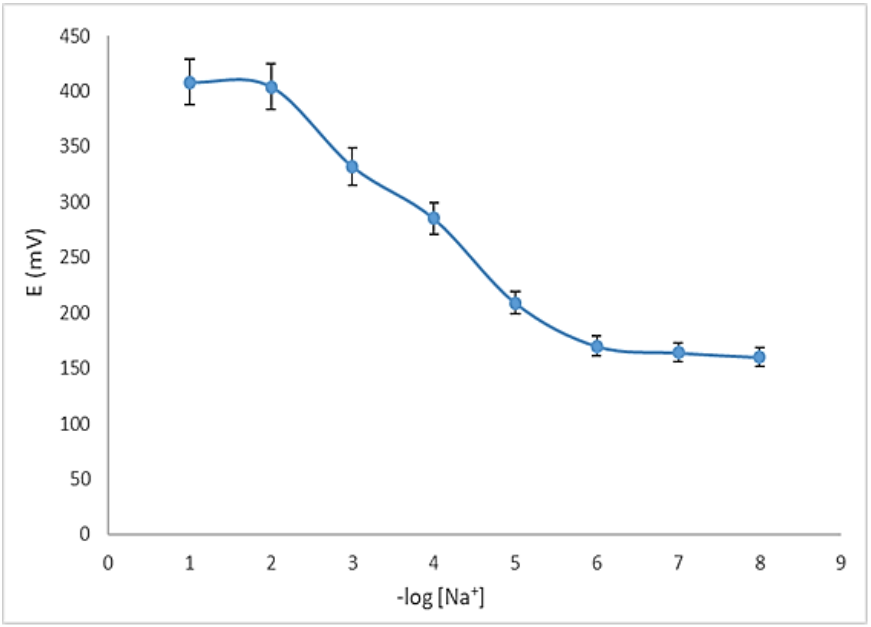

Figure 3: Description of slope performance for the target value Na^+ cation carbon paste electrode under optimized condition

Table 4: The obtained optimum values based on experimental design (design expert software) for desired factors

Factors	Optimum amount
Ionic Liquid	11.40
Paraffin	13.34
Ligand (Ionophore)	3.21
Nanosheets	2.16
Graphite	69.9007
Slope	50.1001

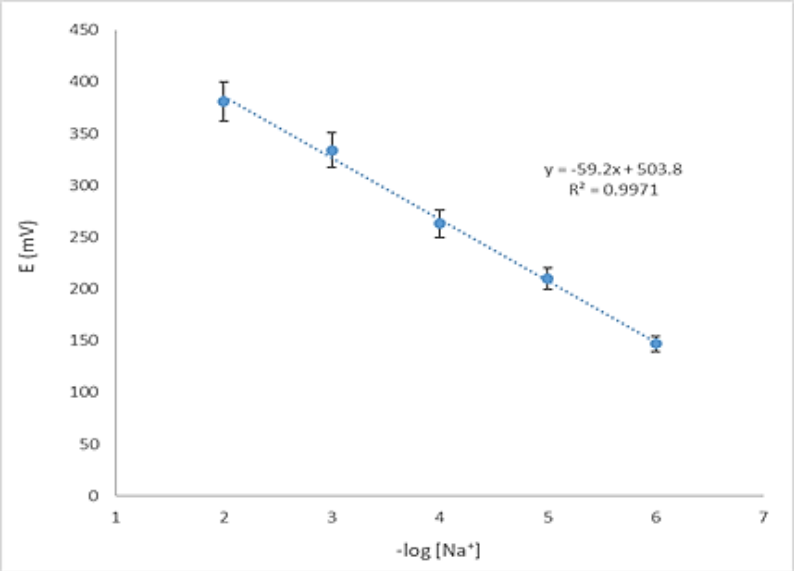

Figure 4: Description of slope performance for the target value Na^+ cation carbon paste electrode under optimized conditions

Reproducibility of the fabricated electrode

Three similar fabricated electrodes under optimization composite were utilized to investigate the reproducibility of the electrode. Then, the calibration curve was plotted for the standard solution of sodium ion within the range of 10^{-6}-10^{-2} mol L^{-1} for the CPE electrode with the optimum percentage of components. Finally, the average slope of the calibration curve was obtained as 59.23 ± 0.16 mV $decade^{-1}$ (Figure 5). The results confirm a Nernstian response of the prepared electrodes under the optimized conditions obtained from the response surface design strategy.

Effect of pH on the electrode response

One of the critical factors in the potentiometric response of the modified electrodes is the pH measurement since there is a competition between the proton and the metal to bind to carrier receptors in the carbon paste structure. The effect of PH on the Nernstian response of a modified and optimized CPE was investigated by applying two concentrations of 10^{-2} mol L^{-1} and 10^{-3} mol L^{-1} sodium nitrate. The pH of the sample solution was changed within a range of 2 to 11 via hydrochloric acid and potassium hydroxide with a concentration of 0.1 mol L^{-1}. The obtained results are shown in Figure 6, showing that the optimum electrode potential response was constant within the pH range of 4-8; as a result, OH^- and H_3O^+ ions did not interfere. Therefore, the desired electrode can be applied within this constant pH range. Out of this range, there is a deviation of potential. It can be related to the competition of H^+ ions, the formation of sodium hydride at pH lower than 4, the instability of the CPE, and the formation of

sodium hydroxide complex in the solution at pH higher than 8.

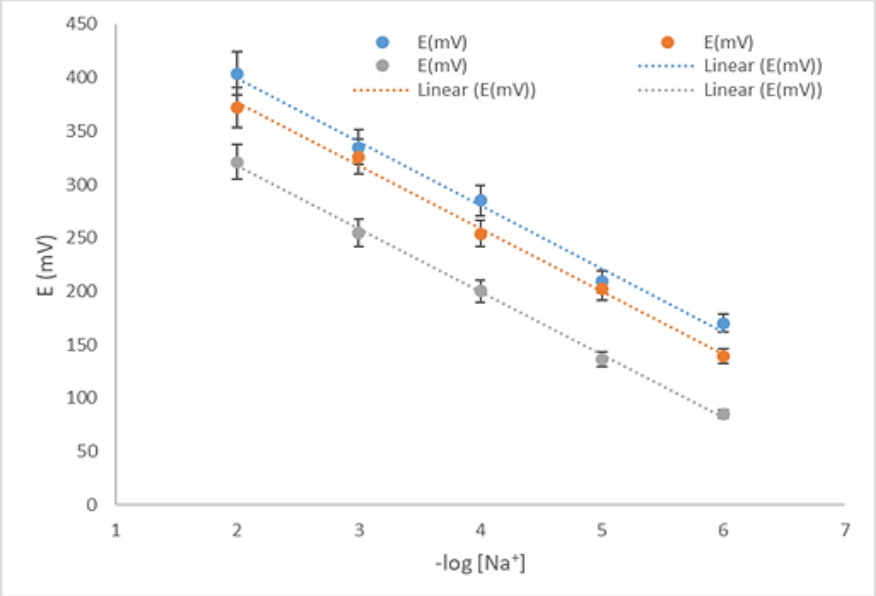

Figure 5: Reproducibility of three similar Na^+ ion CPEs under optimized conditions

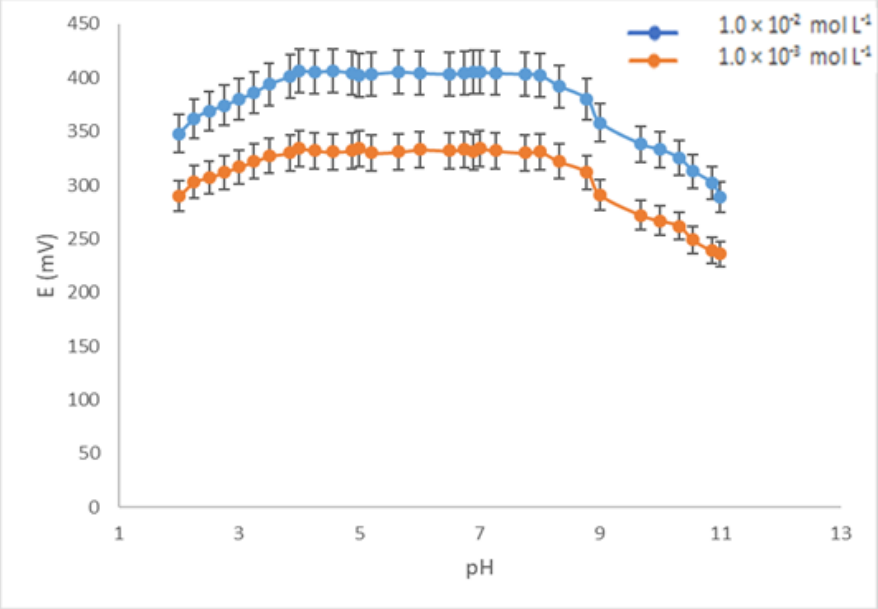

Figure 6: Effect of pH on the potential response of the Na^+ cation CPE at 1×10^{-3} mol·L^{-1} and 1×10^{-2} mol·L^{-1} Na^+ ion under optimized conditions

Electrode selectivity

One of the essential properties of an electrode is its selectivity behaviour which represents the ability to measure the target sample accurately. Selectivity is the efficiency of an electrode in determining the ion in the presence of other disturbing ions. In this study, the selectivity coefficient for the corresponding electrode was determined using the separate solution method (SSM) [36]. The effect of interfering ions on the response of the electrodes is determined by the selectivity coefficient ($K^{pot}_{A,\ B}$). The selectivity coefficients of electrodes are investigated using

different methods, each of which has characteristic constraints. For measuring the selection coefficients, a concentration of 1.0×10^{-3} mol L^{-1} of Na^{+} ion and a concentration of 1.0×10^{-3} mol L^{-1} of interfering ions were considered. The results are shown in Table 5. The result indicates that other cations have a non-significant effect on the performance of optimum CPEs for determining sodium ions. Therefore, the optimum electrode has a high selectivity toward sodium ions.

Dynamic response time and lifetime of fabricated electrode

The dynamic response time is the time required for the electrode to reach the equilibrium potential and stable potential response within the range of ±1 mV of the final potential. When the electrode is consecutively placed into the sample solution from the lower concentration to the higher concentration solution. The rate of electrode potential response stabilization is correlated with the time required to balance the sodium ions in the sample solution and the sodium ions at specific locations in the ligand used in the electrode composition. In the present work, the response time of the corresponding electrode was tested against Na^{+} ion with a concentration in the range of 1×10^{-6}-1×10^{-2} mol L^{-1}. Sodium solutions, each with a difference of ten times of concentration, were studied sequentially. The response time was obtained as 20 Sec (Figure 7). Also, the lifetime of the sensor was monitored for eight consecutive weeks. Until six consecutive weeks, no significant changes were observed in the Nernstian response of the electrode, and it can be used for analytical applications.

Response time of the electrode

The response time is one of the essential parameters for the analytical application of CPEs. The present work investigated the time required to achieve a stable response for sodium solution at concentrations 10^{-6}-10^{-2} mol L^{-1}. The results in Figure 8 indicate that the electrode response is fixed after 20 Sec.

Table 5: Potentiometric selectivity coefficient values of the Na^{+} cation CPE under optimized conditions

interference ions	K SSM	interference ions	K SSM
k^{+}	5.35×10^{-5}	Li^{+}	8.64×10^{-2}
NH_4^{+}	5.49×10^{-3}	Ba^{2+}	2.98×10^{-4}
Sr^{2+}	6.83×10^{-4}	Zn^{2+}	3.76×10^{-7}
Mn^{2+}	1.63×10^{-5}	Cd^{2+}	4.60×10^{-4}
Cs^{1+}	3.27×10^{-6}	Sn^{2+}	1.91×10^{-3}
Co^{2+}	5.20×10^{-7}	Fe^{3+}	4.98×10^{-5}
Ni^{2+}	2.46×10^{-6}	Cr^{3+}	5.71×10^{-5}
AL^{3+}	3.20×10^{-3}	Ca^{2+}	1.2×10^{-6}

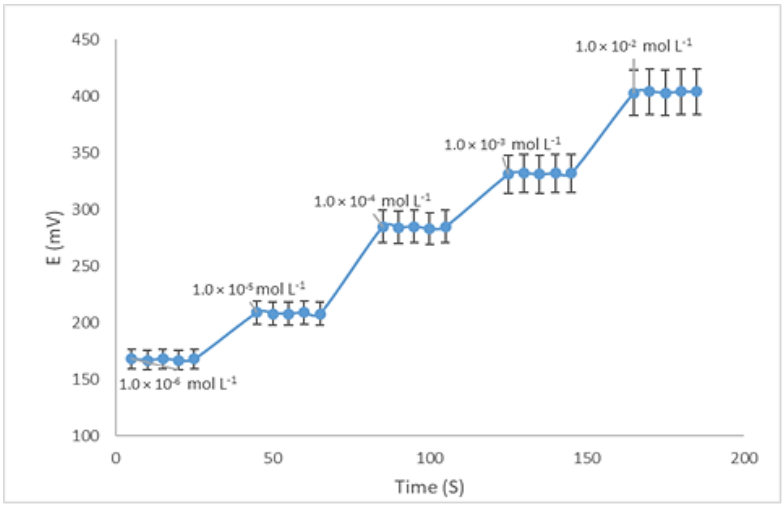

Figure 7: Dynamic response time plot for the Na^+ cation CPE in optimized conditions for different concentrations of sodium cation

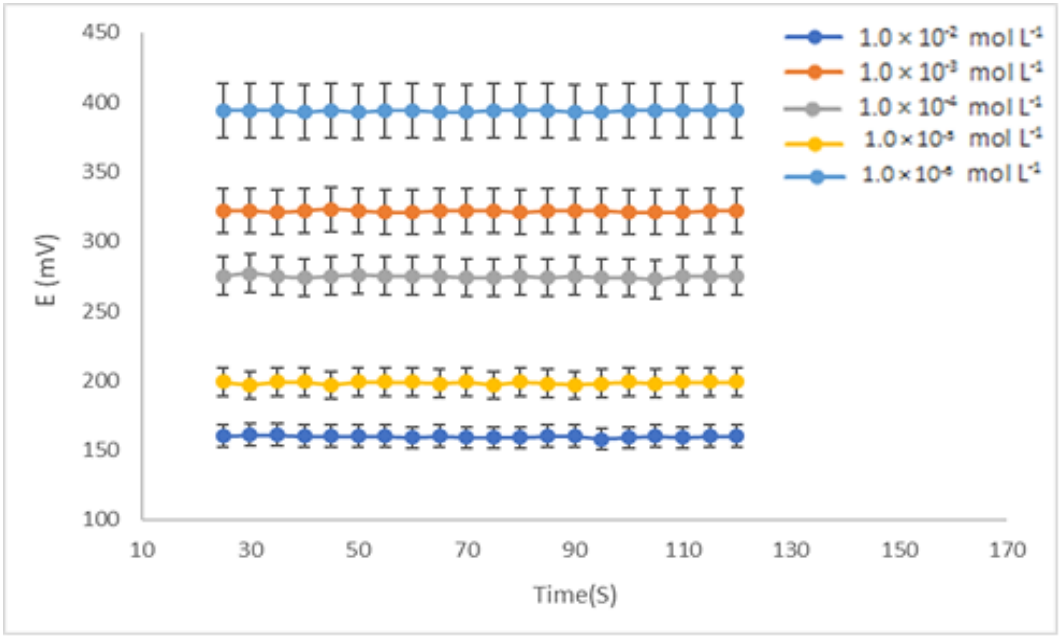

Figure 8: Static potential time plots for the Na^+ cation CPE in the optimized conditions from different concentrations of sodium cation

Application

Several urban water samples were tested to investigate the efficiency of the optimized carbon paste electrode. Urban water samples were obtained from different areas in Mashhad and its suburbs (Mashhad, Iran). All samples were analyzed using the prepared sensor without any sample preparation procedure. The concentration of Na^+ was determined using the calibration method. The results were compared with those obtained by the atomic absorption spectroscopy method for more assurance. The working urban solutions were prepared by diluting the urban sample in distilled water. All experiments were carried out at 22±0.5 °C and repeated triplicate under the same conditions (Table 6). The results confirmed that the electrode could be successfully used to measure sodium ions in real water samples, which are not significantly different from the results obtained with AAS.

Table 6: Results of sodium analysis in urban water samples by the Na^+ cation CPE and reference method (n=3)

Sample	ISE[a] (mg L^{-1})	AAS[a] (mg L^{-1})
urban water 1	2.35	2.40
urban water 2	2.41	2.39
urban water 3	3.20	3.28

[a] *Results are average of triplicate measurements*

DFT calculations

One or two neutral molecules of 1, 4 Diaminoanthraquinone (DAQ) can coordinate with the Na^+ ion, whose optimized geometries are shown in Figure 9. Meanwhile, the 1, 4 Diaminoanthraquinone (DAQ) can be deprotonated firstly to produce its anionic form. Geometries of the neutral molecule of the 1, 4 Diaminoanthraquinone (DAQ) and its anionic form are shown in Figure 10.

One or two anionic molecules of the deprotonated-1,4 Diaminoanthraquinone (DAQ) can link to the Na^+ ion too. The optimized geometries for coordination of the anionic moieties to the Na^+ cation is shown in Figure 11. As seen, the anion is coordinated to the metal ion via the oxygen atom of the carbonyl group and nitrogen atom of the deprotonated amine group, as the deprotonated-1, 4 Diaminoanthraquinone (DAQ) acts as a bidentate ligand. This model has been proposed for the interaction of the deprotonated-1, 4 Diaminoanthraquinone (DAQ) molecule with several metal ions [37].

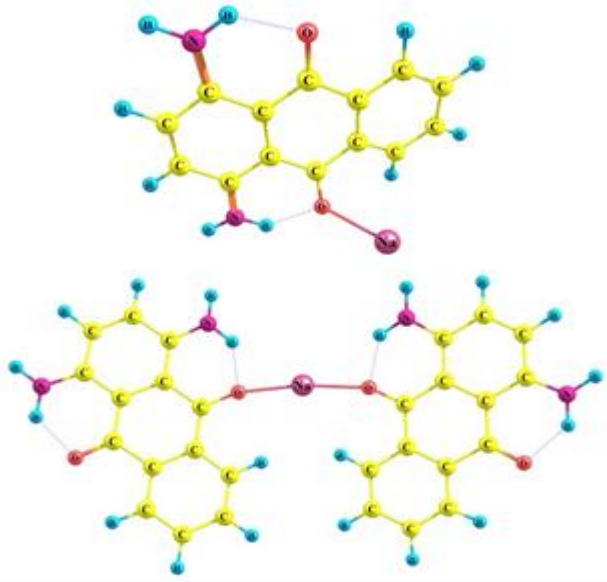

Figure 9: Optimized geometries for coordination of one or two neutral molecules of the 1, 4 Diaminoanthraquinone (DAQ) to the Na^+ cation

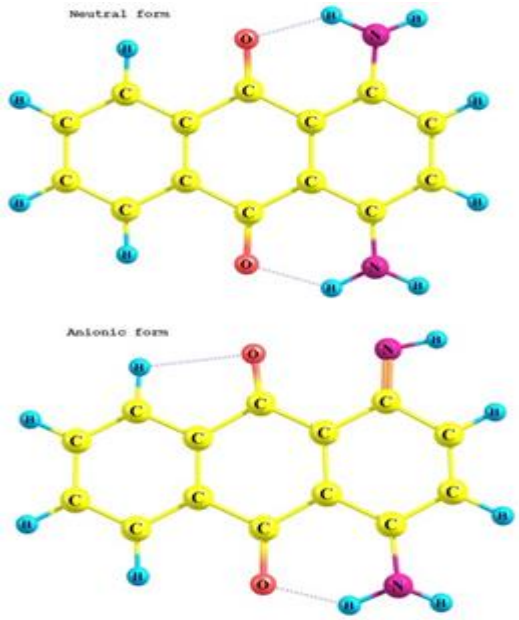

Figure 10: Optimized geometries of the neutral and anionic forms of the 1, 4 Diaminoanthraquinone (DAQ)

The difference in the Gibbs free energies between the products and reactants is known as ΔG. The calculated ΔGs for the investigated-coordination reactions are reported in Table 7. Based on the calculated ΔGs, coordination of two deprotonated-1, 4 Diaminoanthraquinone (DAQ) (its anionic form) to the sodium cation is the most favorable interaction. This complexation involves the most negative value of the ΔG. In the neutral form, the 1, 4 Diaminoanthraquinone (DAQ) molecule coordinates weakly to the Na^+ ion via the oxygen atom of the carbonyl group. However, in the anionic form, the investigated ligand is strongly coordinated to the Na^+ cation *via* two donor atoms. Coordination of the deprotonated-amine nitrogen and carbonyl oxygen to the Na^+ ion results in chelation. The chelating effect causes a very negative ΔG. The chelate formation increases the entropy of the reaction, thereby causing very negative ΔG of the complex formation. Coordination of two deprotonated-1, 4 Diaminoanthraquinone (DAQ) and formation of two chelate rings result in more negative ΔG of the complex formation. Note that the formed complex has a square planar geometry. Two deprotonated nitrogens and two oxygen atoms of the carbonyl groups occupy four positions of the square structure.

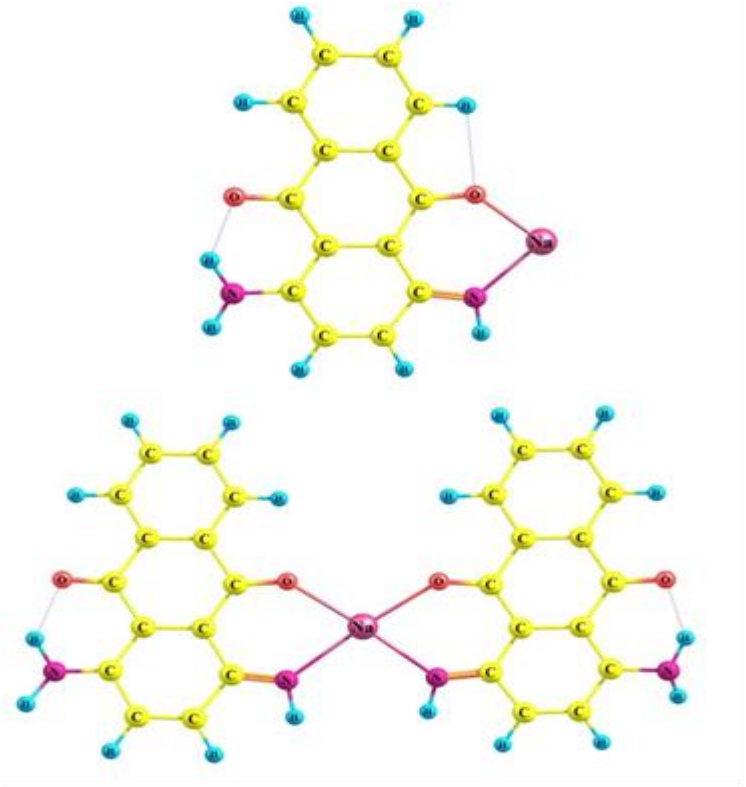

Figure 11: Optimized geometries for coordination of one or two deprotonated 1, 4 Diaminoanthraquinone (DAQ) ligand to the Na^+ cation

Comparison the sensor with other prepared sensors

Several sensors were selected to evaluate the prepared sensor's ability to determine the sodium ion. The results are shown in Table 8. The important advantages of this modified sensor with the previously published paper for sodium-ion determination include the reduction of detection limit, the improvement of dynamic linear range, and the proximity of the slope to the theoretical Nernstian slope. Besides, the sensor has a wider linear range than the other prepared sensors.

Table 7: The ΔG (kJ.mol^{-1}) calculated for complexation of the 1, 4 Diaminoanthraquinone (DAQ) and Na^+ ion in four different positions

Complexation reaction	$\Delta G_{complexation}$
Na^+ - one 1,4-diaminoanthraquinone neutral molecule	-174.65
Na^+ - two 1,4-diaminoanthraquinone neutral molecule	-283.18
Na^+ - one 1,4-diaminoanthraquinone anionic form	-658.10
Na^+ - two 1,4-diaminoanthraquinone anionic form	-888.72

\

Table 8: Comparison of the sensor ability with other prepared sensors

No	Method	Slope mV decade^{-1}	Linear range mol L^{-1}	Detection limit mol L^{-1}	Reference
1	POT-ISE$_S$	59.2 ±0.16	10^{-6} -10^{-2}	8.97 ×10^{-7}	This work
2	POT-CCF	59.2 ± 0.6	10^{-3} -10^{-1}	-	[38]
3	POT-ISE$_S$	56.2 ± 1.4	10^{-4} - 10^{0}	4.0 × 10^{-4}	[39]
4	POT-ISE$_S$	55.1 ± 0.7	10^{-4} -10^{-1}	-	[40]
5	POT(SS-ISE)	58.68	10^{-6} -10^{-1}	-	[41]
6	POT(SS-ISE)	58 ± 3	7.08×10^{-7} -1	3.16 × 10^{-6}	[42]
7	Wireless- ISE	56.1	10^{-4} -1	-	[43]
8	Wireless- ISE	63.75	10^{-4} -10^{-1}	-	[44]
9	Wireless- ISE	54.85 ±5.8	10^{-4} -10^{-1}	-	[45]
10	POT(SS-ISE)	52.4	10^{-4} -1	-	[46]
11	EPADs	54.8±1.4	10^{-3} -1	-	[47]

Conclusion

The present study developed an efficient and fast potentiometric sensor to determine sodium ions in real water samples. The experimental design approach was used to optimize the percentage of components for constructing a new carbon paste electrode instead of one factor at the time strategy. Usage of this procedure offers several important advantages, such as saving cost and time, reducing the number of experiments, getting an accurate response, and examining the effect of independent variables. The optimal conditions, maximum Nernstian slope of the calibration curve, and significant interactions between factors were obtained using the central composite design method based on RSM. The proposed carbon paste electrode was constructed with 1-Hexyl-3methyl imidazolium hexafluorophosphate as an ionic liquid, 1, 4 Diaminoanthraquinone (DAQ) as an ionophore, graphene oxide nanosheets, and paraffin oil as a binder and provided an attractive choice for the determination of Na+ cation using the potentiometric method. The optimum percentages of paraffin, ionic liquid, ionophore, and graphene oxide to prepare the sensor were 13.34, 11.40, 3.21, and 2.16 %, respectively. The sensor displays a stable response time, wide dynamic concentration range (10-6-10-2 mol L-1), good sensitivity, and low detection limit (8.97×10-7 mol L-1) to determine sodium ions. Therefore, the sensor is appropriate for measuring the concentration of Na+ cation in water samples without the effect of interfering with other cations and without the need for any sample preparation procedure such as extraction, derivatization, or filtration steps for real water analysis. This electrode has a fast response time (~20 Sec) over the whole concentration range within the pH range of 4-8 and excellent selectivity coefficients over a range of interfering cations. The electrode could also be used for six consecutive weeks without altering the response. The reproducibility of the sensor under optimized conditions was examined, and it was successfully used as an indicator electrode to measure trace amounts of sodium ions in real water samples.

Acknowledgements

The authors would like to thank the Islamic Azad University of Mashhad, Mashhad, Iran, for financial support.

Funding

This research did not receive any specific grant from funding agencies in the public, commercial, or not-for-profit sectors.

Authors' contributions

All authors contributed to data analysis, drafting, and revising of the paper and agreed to be responsible for all the aspects of this work.

Conflict of Interest

There are no conflicts of interest in this study.

ORCID

Mahmoud Ebrahimi

https://orcid.org/0000-0002-5974-1853

References

[1]. Sharma V., Jayaprakas G.K., Fabrications of electrochemical sensors based on carbon paste electrode for vitamin detection in real samples, Journal of Electrochemical Science and Engineering, 2022, **12**:421 [Crossref], [Google Scholar], [Publisher]

[2]. Pezeshkvar T., Norouzi B., Moradian M., Mirabi A., Synthesis of nickel oxide nanostructures and its application for acyclovir antivirus drug sensing in the presence of sodium dodecyl sulfate, *Ionics*, 2022, **28**:4445 [Crossref], [Google Scholar], [Publisher]

[3]. Adeli A., Khoshnood R.S., Beyramabadi S.A., Pordel M., Morsali A., Multivariate optimization of a novel potentiometric sensor to determine silver ions in real water and pharmacological product samples, *Monatshefte für Chemie-Chemical Monthly*, 2022, **153**:227 [Crossref], [Google Scholar], [Publisher]

[4]. Fanjul-Bolado P., Hernández-Santos D., Lamas-Ardisana P.J., Martín-Pernía A., Costa-García A., Electrochemical characterization of screen-printed and conventional carbon paste electrodes, *Electrochimica Acta*, 2008, **53**:3635 [Crossref], [Google Scholar], [Publisher]

[5]. Sherino B., Mohamad S., Abdul Halim S.N.A., Abdul Manan N.S., Electrochemical detection of hydrogen peroxide on a new microporous Ni–metal organic framework material-carbon paste electrode, *Sensors and Actuators B: Chemical*, 2018, **254**:1148 [Crossref], [Google Scholar], [Publisher]

[6]. Shahamirifard S.A., Ghaedi M., A new electrochemical sensor for simultaneous determination of arbutin and vitamin C based on hydroxyapatite-ZnO-Pd nanoparticles modified carbon paste electrode, *Biosensors and Bioelectronics*, 2019, **141**:111474 [Crossref], [Google Scholar], [Publisher]

[7]. Manasa G., Bhakta A.K., Mekhalif Z., Mascarenhas R.J., Bismuth-nanoparticles decorated multi-wall-carbon-nanotubes cast-coated on carbon paste electrode; an electrochemical sensor for sensitive determination of Gallic Acid at neutral pH, *Materials Science for Energy Technologies*, 2020, **3**:174 [Crossref], [Google Scholar], [Publisher]

[8]. Ghanbari M.H., Shahdost-Fard F., Rostami M., Khoshroo A., Sobhani-Nasab A., Gholipour N., Salehzadeh H., Ganjali M.R., Rahimi-Nasrabadi M., Ahmadi F., Electrochemical determination of the antipsychotic medication clozapine by a carbon paste electrode modified with a nanostructure prepared from titania nanoparticles and copper oxide, *Microchimica Acta*, 2019, **186**:698 [Crossref], [Google Scholar], [Publisher]

[9]. Madhuchandra H.D., Swamy B.E.K., Electrochemical determination of Adrenaline and Uric acid at 2-Hydroxybenzimidazole modified carbon paste electrode Sensor: A voltammetric study, *Materials Science for Energy Technologies*, 2020, **3**:464 [Crossref], [Google Scholar], [Publisher]

[10]. Pourtaheri E., Taher M.A., Beitollahi H., Synergistic signal amplification based on ionic liquid-$BaTiO_3$ nanoparticle carbon paste electrode for sensitive voltammetric determination of acetaminophen, *Analytical and Bioanalytical Chemistry Research*, 2018, **5**:261 [Crossref], [Google Scholar], [Publisher]

[11]. Tajik S., Lohrasbi-Nejad A., Mohammadzadeh Jahani P., Askari M.B., Salarizadeh P., Beitollahi H., Co-detection of carmoisine and tartrazine by carbon paste electrode modified with ionic liquid and MoO_3/WO_3 nanocomposite, *Journal of Food Measurement and Characterization*, 2022, **16**:722 [Crossref], [Google Scholar], [Publisher]

[12]. Hernández-Vargas S.G., Cevallos-Morillo C.A., Aguilar-Cordero J.C., Effect of ionic liquid structure on the electrochemical response of dopamine at room temperature ionic liquid-modified carbon paste electrodes (IL-CPE), *Electroanalysis*, 2020, **32**:1938 [Crossref], [Google Scholar], [Publisher]

[13]. Báez C., Navarro F., Fuenzalida F., Aguirre M.J., Arévalo M.C., Afonso M., García C., Ramírez G., Palenzuela J.A., Electrical and Electrochemical Behavior of Carbon Paste Electrodes Modified with Ionic Liquids Based in N-Octylpyridinium Bis (Trifluoromethylsulfonyl) Imide. A Theoretical and Experimental Study, *Molecules,* 2019, **24**:3382 [Crossref], [Google Scholar], [Publisher]

[14]. Šekuljica S., Guzsvány V., Anojčić J., Hegedűs T., Mikov M., Kalcher K., Imidazolium-based ionic liquids as modifiers of carbon paste electrodes for trace-level voltammetric determination of dopamine in pharmaceutical preparations, *Journal of Molecular Liquids*, 2020, **306**:112900 [Crossref], [Google Scholar], [Publisher]

[15]. Firouzi M., Giahi M., Najafi M., Homami S.S., Mousavi S.H.H., Electrochemical determination of amlodipine using a CuO-NiO nanocomposite/ionic liquid modified carbon paste electrode as an electrochemical sensor, *Journal of Nanoparticle Research*, 2021, **23**:82 [Crossref], [Google Scholar], [Publisher]

[16]. Ray M., Sports Drinks & Energy Drinks: Comparison on Physico-chemical parameters, Bulk Metals and Nitrate Ions, *Bulletin Monumental Journal*, 2021, **22**:105 [Google Scholar], [Publisher]

[17]. (a) Banik S., Acid-Base Imbalance, Transfusion Practice in Clinical Neurosciences, *Springer*, 2022, 215-224 [Crossref], [Google Scholar], [Publisher] (b) Sengar M., Saxena S., Satsangee S., Jain R., Silver nanoparticles decorated functionalized multiwalled carbon nanotubes modified screen printed sensor for the voltammetric determination of butorphanol, *Journal of Applied Organometallic Chemistry*, 2021, **1**:95 [Crossref], [Google Scholar], [Publisher]

[18]. Palmer B.F., Kelepouris E., Clegg D.J., Renal tubular acidosis and management strategies: a narrative review, *Advances in Therapy*, 2021, **38**:949 [Crossref], [Google Scholar], [Publisher]

[19]. Pohl H.R., Wheeler J.S., Murray H.E., Sodium and potassium in health and disease, Interrelations between essential metal ions and human diseases, *Springer,* 2013, 29-47 [Google Scholar]

[20]. Łabno-Kirszniok K., Kujawa-Szewieczek A., Wiecek A., Piecha G., The Effects of Short-Term Changes in Sodium Intake on Plasma Marinobufagenin Levels in Patients with Primary Salt-Sensitive and Salt-Insensitive Hypertension, *Nutrients*, 2021, **13**:1502 [Crossref], [Google Scholar], [Publisher]

[21]. Banerjee P., Prasad B., Determination of concentration of total sodium and potassium in surface and ground water using a flame photometer, *Applied Water Science*, 2020, **10**:113 [Crossref], [Google Scholar], [Publisher]

[22]. Shammi M., Rahman M.M., Bodrud-Doza M., Impacts of Salinity Intrusion in Community Health: A Review of Effectiveness of Adaptation Measures to Decrease Drinking Water Sodium (DWS) from Coastal Areas of Bangladesh, *Healthcare,* 2019, **7**:50 [Crossref], [Google Scholar], [Publisher]

[23]. A) Ghorbani M., Ariavand S., Aghamohammadhasan M., Seyedin O., Synthesis and optimization of a green and efficient sorbent for removal of three heavy metal ions from wastewater samples: kinetic, thermodynamic, and isotherm studies, *Journal of the Iranian Chemical Society,* 2021, **18**:1947 [Crossref], [Google Scholar], [Publisher] (b) Allahresani A., Ghorbanian F., Nasseri M., Kazemnejadi M., Isolation and Characterization of Bis(2-Ethylheptyl) Phthalate from Cynodon Dactylon (L.) and Studies on the Catalytic Activity of its Cu(II) Complex in the Green Preparation of 1,8-Dioxo-Octahydroxanthenes, *Journal of Applied Organometallic Chemistry*, 2022, **2**:140 [Crossref], [Google Scholar], [Publisher] (c) Kamble R., Gaikwad M., Tapare M., Hese S., Kadam S., Ambhore A., Dawane B., DTP/SiO_2: An Efficient And Reusable Heterogeneous Catalyst For synthesis of dihydropyrano[3,2-c]chromene-3-carbonitrile derivatives, *Journal of Applied Organometallic Chemistry*, 2021, **1**:22 [Crossref], [Google Scholar], [Publisher]

[24]. (a) Saljooqi A., Shamspur T., Mostafavi A., The electrochemical sensor based on graphene oxide nanosheets decorated by gold nanoparticles and polythiophene for nicotine sensing in biological samples and cigarette, *Journal of*

Materials Science: Materials in Electronics, 2020, **31**:5471 [Crossref], [Google Scholar], [Publisher] (b) Shayegan H., Safari Fard V., Taherkhani H., Rezvani M., Efficient removal of cobalt(II) ion from aqueous solution using amide-functionalized metal-organic framework, *Journal of Applied Organometallic Chemistry*, 2022, **2**:109 [Crossref], [Google Scholar], [Publisher]

[25]. Govindasamy M., Wang S.F., Subramanian B., Ramalingam R.J., Al-lohedan H., Sathiyan A., A novel electrochemical sensor for determination of DNA damage biomarker (8-hydroxy-2′-deoxyguanosine) in urine using sonochemically derived graphene oxide sheets covered zinc oxide flower modified electrode, *Ultrasonics Sonochemistry*, 2019, **58**:104622 [Crossref], [Google Scholar], [Publisher]

[26]. Ghorbani M., Pedramrad T., Aghamohammadhasan M., Seyedin O., Akhlaghi H., Lahoori N.A., Simultaneous clean-up and determination of Cu(II), Pb(II) and Cr(III) in real water and food samples using a magnetic dispersive solid phase microextraction and differential pulse voltammetry with a green and novel modified glassy carbon electrode, *Microchemical Journal*, 2019, **147**:545 [Crossref], [Google Scholar], [Publisher]

[27]. (a) Heravizadeh O.R., Khadem M., Dehghani F., Shahtaheri S.J., Determination of fenthion in urine samples using molecularly imprinted nanoparticles: modelling and optimisation by response surface methodology, *International Journal of Environmental Analytical Chemistry*, 2020, 1 [Crossref], [Google Scholar], [Publisher] (b) Ahmadi Y., Alami S., Hatefi N., Efficient Synthesis of Bis(3-Methylphenyl)Sulfoxide Aza Macrocycles from a Bis(3-Methylphenyl)Sulfoxide Diester and Diamine Derivatives, *Journal of Applied Organometallic Chemistry*, 2022, **2**:173 [Crossref], [Google Scholar], [Publisher] (c) Pund G.B., Dhumal S.T., Hebade M.J., Farooqui M., Dobhal, B.S., Meglumine Catalysed Green Synthesis of Ethyl-6-amino-5-cyano-2-methyl-4-phenyl-4H-pyran-3-carboxylate Derivatives, *Journal of Applied Organometallic Chemistry*, 2022, **2**:15 [Crossref], [Google Scholar], [Publisher] (d) Anafcheh M., A comparison between density functional theory calculations and the additive schemes of polarizabilities of the Li-F-decorated BN cages, *Journal of Applied Organometallic Chemistry*, 2021, **1**:125 [Crossref], [Google Scholar], [Publisher]

[28]. Ghorbani M., Mohammadi P., Keshavarzi M., Saghi M.H., Mohammadi M., Shams A., Aghamohammadhasan M., Simultaneous determination of organophosphorus pesticides residues in vegetable, fruit juice, and milk samples with magnetic dispersive micro solid-phase extraction and chromatographic method; Recruitment of simplex lattice mixture design for optimization of novel sorbent composites, *Analytica Chimica Acta*, 2021, **1178**:338802 [Crossref], [Google Scholar], [Publisher] (b) Shinde R.A., Adole V.A., Anti-microbial evaluation, Experimental and Theoretical Insights into Molecular Structure, Electronic Properties, and Chemical Reactivity of (E)-2-((1H-indol-3-yl)methylene)-2,3-dihydro-1H-inden-1-one, *Journal of Applied Organometallic Chemistry*, 2021, **1**:48 [Crossref], [Google Scholar], [Publisher] (c) Sharma G., Sharma S., Synthetic Impatienol analogues as potential cyclooxygenase-2 inhibitors: a preliminary study, *Journal of Applied Organometallic Chemistry*, 2021, **1**:66 [Crossref], [Google Scholar], [Publisher]

[29]. Busan R.C., Murphy P.C., Hatke D.B., Simmons B.M., Wind tunnel testing techniques for a tandem tilt-wing, distributed electric propulsion vtol aircraft, *AIAA SciTech 2021 Forum*, 2021, 1189 [Crossref], [Google Scholar], [Publisher]

[30]. Durakovic B., Design of experiments application, concepts, examples: State of the art, *Periodicals of Engineering and Natural Sciences*, 2017, **5**:421 [Crossref], [Google Scholar], [Publisher]

[31]. Lee C., Yang W., Parr R.G., Development of the Colle-Salvetti correlation-energy formula into a functional of the electron density, *Physical Review B*, 1988, **37**:785 [Crossref], [Google Scholar], [Publisher]

[32]. Frisch M.J., Trucks G.W., Schlegel H.B., Gaussion 03 Revision B. 03 [CP], Pittsburgh PA: Goussion, Inc, 2003 [Google Scholar]

[33]. Zhurko G., Zhurko D., ChemCraft, version 1.6, 2009 [Publisher]
[34]. Ghorbani M., Seyedin O., Aghamohammadhassan M., Adsorptive removal of lead (II) ion from water and wastewater media using carbon-based nanomaterials as unique sorbents: A review, *Journal of environmental management*, 2020, **254**:109814 [Crossref], [Google Scholar], [Publisher]
[35]. Rajabi N., Masrournia M., Abedi M., The Evaluation of Optimal Conditions for Constructing of Potentiometric Gadolinium Sensor using Experimental Design, *Analytical Bioanalytical Electrochemistry*, 2019, **11**:1057 [Google Scholar]
[36]. Ali T.A., Mohamed G.C., Said A.H., Construction and Performance Characteristics of Modified Screen Printed and Modified Carbon Paste Sensors for Selective Determination of Cu(II) Ion in Different Polluted Water Samples, *Chemical Engineering Communications*, 2016, **203**:724 [Crossref], [Google Scholar], [Publisher]
[37]. Vijayashree M.N., Subramanyam S.V., Samuelson A.G., High pressure and low temperature conducting properties of organic semiconducting metal-anthraquinones, *Journal of Applied Polymer Science*, 1993, **49**:2171 [Crossref], [Google Scholar], [Publisher]
[38]. Parrilla M., Ferré J., Guinovart T., Andrade F.J., Wearable Potentiometric Sensors Based on Commercial Carbon Fibres for Monitoring Sodium in Sweat, *Electroanalysis*, 2016, **28**:1267 [Crossref], [Google Scholar], [Publisher]
[39]. Stekolshchikova A.A., Radaev A.V., Orlova O.Y., Nikolaev K.G., Skorb E.V., Thin and Flexible Ion Sensors Based on Polyelectrolyte Multilayers Assembled onto the Carbon Adhesive Tape, *ACS Omega*, 2019, **4**:15421 [Crossref], [Google Scholar], [Publisher]
[40]. Wang S., Bai Y., Yang X., Liu L., Li L., Lu Q., Li T., Zhang T., Highly stretchable potentiometric ion sensor based on surface strain redistributed fiber for sweat monitoring, *Talanta*, 2020, **214**:120869 [Crossref], [Google Scholar], [Publisher]
[41]. Paczosa-Bator B., Pięk M., Piech R., Application of Nanostructured TCNQ to Potentiometric Ion-Selective K^+ and Na^+ Electrodes, *Analytical Chemistry*, 2015, **87**:1718 [Crossref], [Google Scholar], [Publisher]
[42]. Roy S., David-Pur M., Hanein Y., Carbon nanotube-based ion selective sensors for wearable applications, *ACS Applied Materials & Interfaces*, 2017, **9**:35169 [Crossref], [Google Scholar], [Publisher]
[43]. Lim H.R., Kim Y.S., Kwon S., Mahmood M., Kwon Y.T., Lee Y., Lee S.M., Yeo W.H., Wireless, Flexible, Ion-Selective Electrode System for Selective and Repeatable Detection of Sodium, *Sensors*, 2020, **20**:3297 [Crossref], [Google Scholar], [Publisher]
[44]. Bandodkar A.J., Molinnus D., Mirza O., Guinovart T., Windmiller J.R., Valdés-Ramírez G., Andrade F.J., Schöning M.J., Wang J., Epidermal tattoo potentiometric sodium sensors with wireless signal transduction for continuous non-invasive sweat monitoring, *Biosensors and Bioelectronics*, 2014, **54**:603 [Crossref], [Google Scholar], [Publisher]
[45]. Alizadeh A., Burns A., Lenigk R., Gettings R., Ashe J., Porter A., McCaul M., Barrett R., Diamond D., White P., Skeath P., Tomczak M., A wearable patch for continuous monitoring of sweat electrolytes during exertion, *Lab on a Chip*, 2018, **18**:2632 [Crossref], [Google Scholar], [Publisher]
[46]. Ghosh T., Chung H.J., Rieger J., All-solid-state sodium-selective electrode with a solid contact of chitosan/prussian blue nanocomposite, *Sensors*, 2017, **17**:2536 [Crossref], [Google Scholar], [Publisher]
[47]. Lan W.J., Zou X.U., Hamedi M.M., Hu J., Parolo C., Maxwell E.J., Bühlmann P., Whitesides G.M., Paper-Based Potentiometric Ion Sensing, *Analytical Chemistry*, 2014, **86**:9548 [Crossref], [Google Scholar], [Publisher]

HOW TO CITE THIS ARTICLE
Shiva Ariavand, Mahmoud Ebrahimi, Ebrahim Foladi. Design and Construction of a Novel and an Efficient Potentiometric Sensor for Determination of Sodium ion in Urban Water Samples. *Chem. Methodol.*, 2022, 6(11) 886-904
https://doi.org/10.22034/CHEMM.2022.348712.1567
URL: http://www.chemmethod.com/article_155298.html